ANITA Note 04-002

****

The ANITA Trigger Logic:
Estimates of Thermal Noise Trigger Rates
and Practical Operating Thresholds

G.S. Varner[a], P.W. Gorham[a,b], A. Jongeling[b] and L.A. White[b]

[a]*University of Hawaii* and [b]*NASA Jet Propulsion Laboratory*

May, 2004

Abstract

This note is intended to document the baseline ANITA trigger logic as of the time of the SMEX CSR. In addition to better defining the logic, this exercise was done as a cross-check on the noise trigger rates for the sensitivity levels assumed in Monte Carlo simulations of the ANITA GZK neutrino reach. Analytical and simulation results are presented which demonstrate an acceptable thermal noise trigger rate while maintaining exquisite signal sensitivity.

1 Trigger Rate Constraints

In order to maximize the GZK neutrino reach of ANITA it is essential to operate as far down into the thermal noise as is feasible. From a practical perspective, this limit is set by the rate for accidental triggers which the data acquisition system can tolerate, as summarized in Table 1. These numbers are based upon expectations at the time of the writing of the Concept Study Report [1].

Waveform sampling rate	3GSa/s
Waveform depth (single LABRADOR buffer)	256 samples
Sampling window (single LABRADOR buffer)	85 ns
Nominal trigger Hold latency	∼50 ns
RF channels	96
Event size	∼36kBytes
Hardware trigger rate maximum	∼5 Hz
Software reduction factor	20
Event recording rate to disk	0.25 Hz

Table 1: ANITA data acquisition parameters and subsequent trigger rate constraints.

Purely noise triggered events contain nothing of interest in the Fourier or time domains, and should be readily removed at the software level. However transferring and processing such noise events does represent a burden on processor resources. Table 1 reflects the expectation of the data reduction power possible and the resource overhead encumbered using a representative FFT algorithm.

2 The RF Trigger Path

An overview of the impulsive RF recording system for ANITA is illustrated schematically in Figure 1. Ultra-high energy neutrino interactions in the ice produce an impulsive radio pulse due to net charge imbalance in the induced electromagnetic shower, as predicted by Askaryan [2]. While locally these transient RF signals are quite intense, for ANITA most of the detection volume is at a distance of many hundreds of kilometers. As a result, in order to maximize sensitivity for observation of these rare events, it is important to operate well into the thermal noise on a per channel basis.
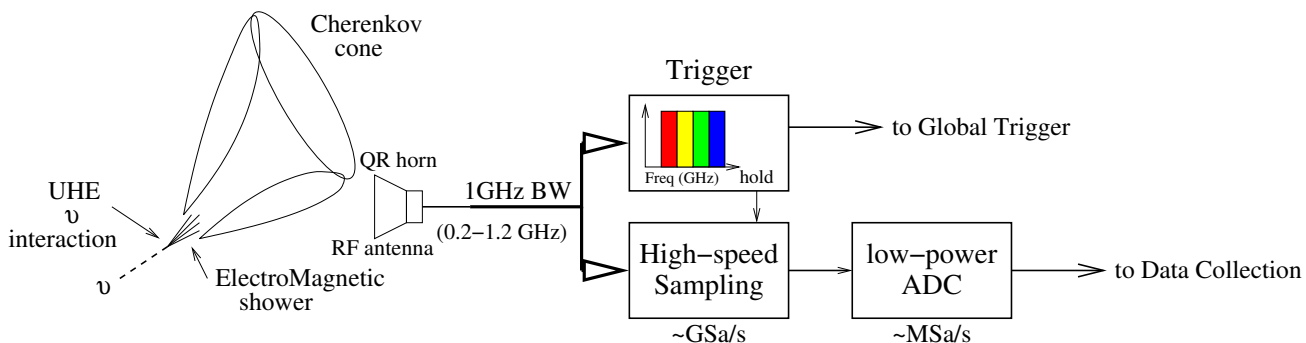

Figure 1: ANITA RF recording and triggering overview.

A strategy for operation in such an environment was established through experience in operating the GLUE [3] experiment, and further evaluated as part of the ANITA-lite prototype mission [4]. Experience teaches that it is essential to have as many independent estimators of signal, in which the noise is statistically independent, as is feasible. In Figure 2 is diagrammed the interaction between the Sampling Unit for RF (SURF) boards, where the elements of Figure 1 are located, and the Trigger Unit for RF (TURF) boards, where the global trigger logic is located. Each SURF board is planned to accomodate RF inputs which corresponds to 4 dual polarization quad ridge horn antennas. For the purposes of triggering, the vertical and horizontal polarizations from each antenna are combined into left and right circular polarizations (LCP, RCP) in each of 4 frequency trigger bands, as described below. In this configuration, there are thus 8 trigger signals available from each antenna to form a trigger. For 4 on-board antennas, this sums to 32 bits of trigger information that are passed from each SURF to the TURF board. Physically the TURF may be a monolithic board, in a single compact PCI (cPCI) crate solution, or a pair of boards in a two crate configuration. In either case, for a baseline configuration of 40 antennas this corresponds to 320 signals from the SURF to TURF. Going from the TURF to the SURF are two types of signal: `Hold` and `Digitize`. Because the sampling window is rather narrow, the latency for making a trigger decision is rather short, on the order of 40-50ns. The deadtime due to a decision to digitize is rather long, on the order of a couple hundred μs. The Switched Capacitor Array (SCA) sampling chip has a feature by which the analog values may be frozen for some time, before a digitization decision
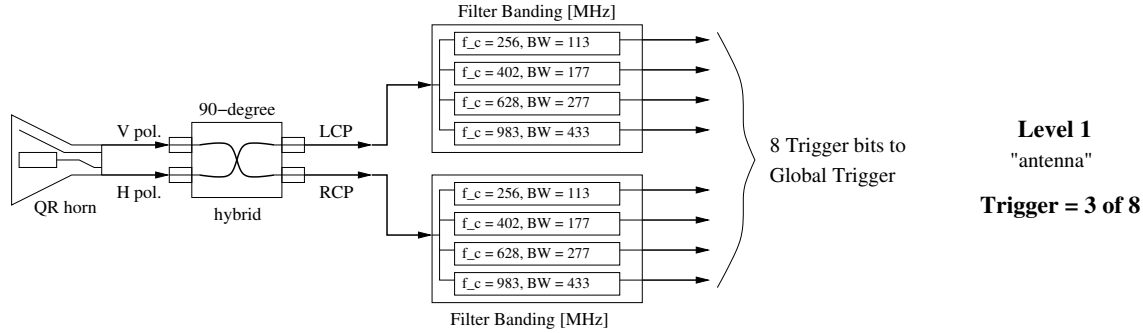
needs to be made. This interval may be used to form a more complex and time consuming analysis of the trigger bits. The `Hold` signal provides this functionality. If after further processing (probably no longer than a few 100ns) no trigger is formed, the `Hold` is released and the waveform sampling continues. Should a trigger be accepted, the `Hold` state continues and a `Digitize` is issued, which starts the analog conversion and data collection cycle. This timing is illustrated in Figure 3. The flow of the trigger logic naturally follows from this two stage approach, combined with the need to possibly exchange information between two separate FPGA processing chips, as discussed in the next subsection.

Figure 2: Sampling Unit for RF (SURF) and Trigger Unit for RF (TURF) block diagram, with the signal flow between them indicated and described in the text.

Figure 3: A timing diagram of ANITA trigger formation and decision making.

3

Figure 4: A diagram of a single antenna trigger path.

2.1 Antenna Trigger Definition Level 1

Figure 4 shows in detail the trigger path signal chain for a given dual polarization quad ridge horn. Vertical and horizontal polarizations are combined for 4 different frequency bands, providing a sum of 8 trigger signals for each antenna. For the purposes of this analysis, it was deemed reasonable that an antenna be considered "hit" if trigger thresholds are exceeded in 3 out of the 8 trigger bits. This is designated a **Level 1** trigger and could be formed either locally (on the SURF) or in the TURF logic. Doing the latter is preferred, as it allows for comparing the hit frequency bands across multiple antennas which could be used to reject narrow-band EMI background.

2.2 Cluster Trigger Definition Level 2

Higher levels of triggering are implemented using the individual antenna bits and the natural 16-fold symmetry of the ANITA antenna array. This symmetry is evident in Figure 5. A second level of trigger combinations are formed by considering coincidences among antennas in clusters, as indicated in the right side of this figure. Designated as **Level 2**, this local clustering is implemented by requiring some number of adjacent antennas be simultaneously hit. The right side of figure 5 illustrates the case of both the top and bottom array of antennas satisfying the **Level 2** criterion, which is 2 of 5 in a given ϕ sector. The requirement for the nadir array is 2 of 3 for **Level 2**, and a different threshold for a standalone trigger, as will be explained below. These **Level 2** triggers are formed quickly and locally and used to implement a prompt `Hold` local to the top, bottom or nadir arrays respectively. This arrangement naturally accomodates the requirements above on latency.

2.3 Global Trigger Definition Level 3

In each of the 16 ϕ sectors, the **Level 2** trigger bits may be logically combined to form a global trigger decision, as illustrated in Figure 6. For the purposes of monitoring and prioritizing these triggers, four possible "`Trigger Types`" are considered. The first three are the logical AND of the top, bottom and nadir **Level 2** bits taken two at a time. A fourth (`Trig Type = 4`) state which can invoke a **Level 3** accept is defined by the state of 3 of 3 of the nadir antennas mapped to the same ϕ sector having a **Level 1** accept. This additional provision is made to improve acceptance for nearby events which cannot be seen by the top or bottom arrays. These conditions and nominal overlap timing widths are summarized in Table 2.

Logical segmentation

(example Trigger Type = 1 shown)

Top cluster
L2 = 2 of 5

Phi = 0
(1 of 16)

Bottom cluster
L2 = 2 of 5
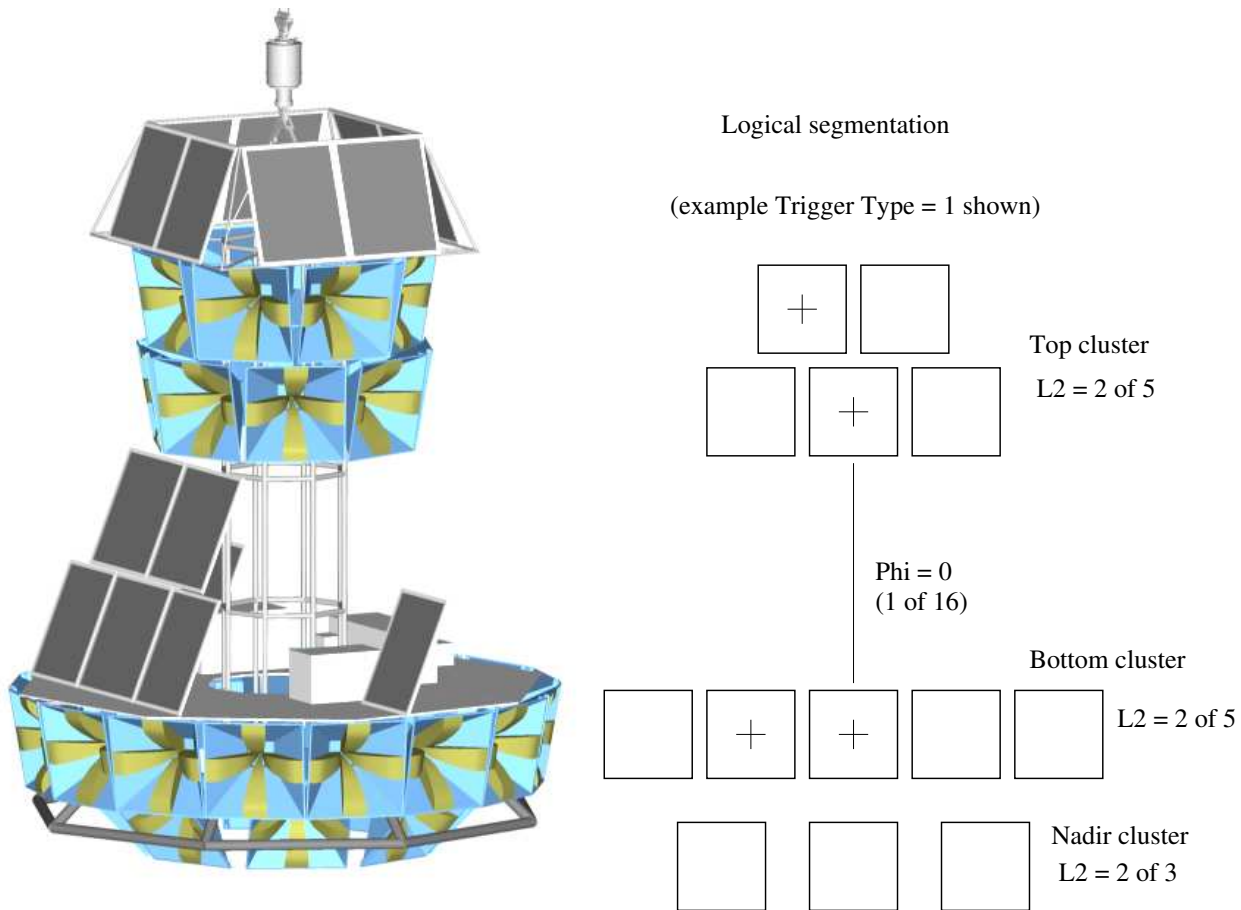
Nadir cluster
L2 = 2 of 3

Figure 5: Physical partitioning and definition of global trigger segments is based upon the 16-fold symmetry of the ANITA antenna array, as seen on left. Each of these 22.5° sectors is referenced as a ϕ trigger element in the text. On the right is a sample of the trigger geometry considered for each ϕ sector.
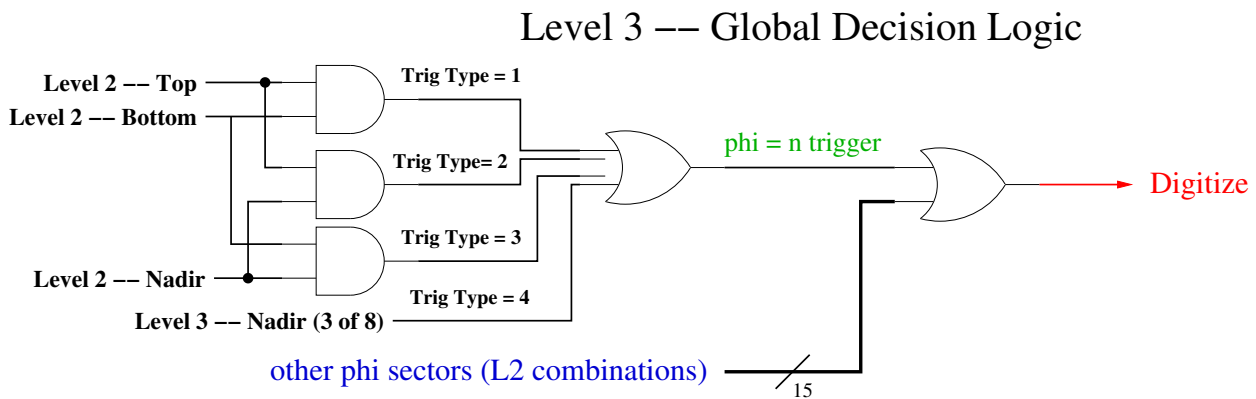
Level 3 –– Global Decision Logic

Level 2 –– Top
Level 2 –– Bottom

Trig Type = 1

Trig Type= 2

phi = n trigger

Digitize

Trig Type = 3

Level 2 –– Nadir
Level 3 –– Nadir (3 of 8)

Trig Type = 4

other phi sectors (L2 combinations)

15

Figure 6: An illustration of the multi-level trigger scheme for ANITA.

ANITA Trigger Level	Logical Combinatorics	Timing Window	Comments
Level 1	3 of 8	20ns	per antenna
Level 2 – top, bottom	2 of 5	20ns	per ϕ segment
Level 2 – nadir	2 of 3	20ns	per ϕ segment
Level 3 – Type 1	**L2** top AND **L2** bottom	50ns	by ϕ segment
Level 3 – Type 2	**L2** top AND **L2** nadir	50ns	by ϕ segment
Level 3 – Type 3	**L2** bottom AND **L2** nadir	50ns	by ϕ segment
Level 3 – Type 4	3 of 3 in ϕ of **L1** nadir	20ns	nadir stand-alone

Table 2: A summary of ANITA trigger level definitions.

3 Analysis of Trigger Rates

In order to understand and confirm thermal noise trigger rates, it is important to model the random coincidences that the logic described above generates. For the most part this can be done analytically. However there are two issues that a simple calculation of binomial coincidence probabilities doesn't correctly model in the ANITA system: the diode detector response, and the correlations between antenna hits in ϕ sectors. These are addressed in estimates of each of the trigger levels below. A full Monte Carlo program has been developed [5] to model this. Comparison is made with simple analytical calculations, demonstrating good agreement.

3.1 Single antenna rates – Level 1

Somewhat of a disconnect exists here in that the values simulated in the neutrino sensitivity MC are stated in noise voltage σ values. However, as may be seen in Figure 7, the direct observable at the discriminator input, characterized as the ratio of Power over average Power, is complicated and not yet properly modelled. This does not imply that the characteristic response of this device cannot be modelled, and if fact power fluctuations due purely to stationary, white and Gaussian noise can be modelled as an exponential distribution, as indicated in Figure 7. Mathematically these two quantities may be related as:

$$P = \frac{\sigma^2}{2} + ln\left(\frac{\sqrt{2}}{2}\sigma\right) \tag{1}$$

and the inverse, which is illustrated in Figure 8:

$$\sigma = \sqrt{2P - ln(\pi \cdot P)}. \tag{2}$$

Obviously a realistic modelling of the trigger banding and the actual diode response will modify this simple correlation plot. An effort is under way to better model this. For the purposes of this exercise, noise fluctuations are modelled on this a simple exponential distribution and the thresholds will be characterized in units of the Power normalized to the average Power: `Power/(average Power)`. The rate at which each single channel will be triggering due to thermal fluctuations as a function of this threshold unit is shown in Figure 9.
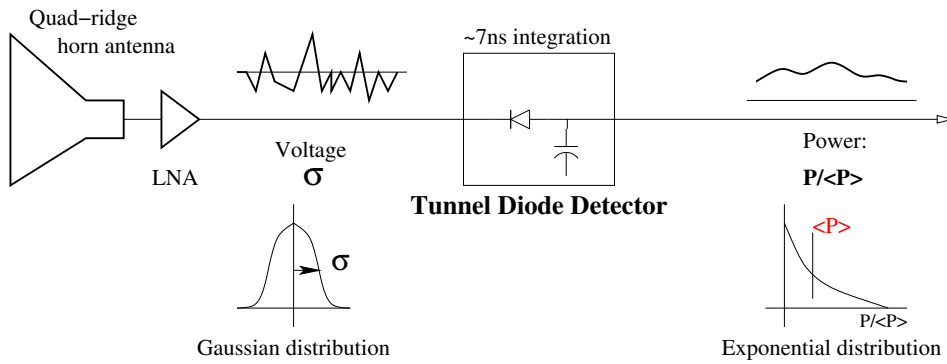
Figure 7: Schematic representation of the correspondence of the input voltage noise and the subsequent integrated power output from the tunnel diode detector. As indicated, while the thermal noise fluctuations may be modelled as a Gaussian distribution, the output of the diode detector is modelled as an exponential distribution.
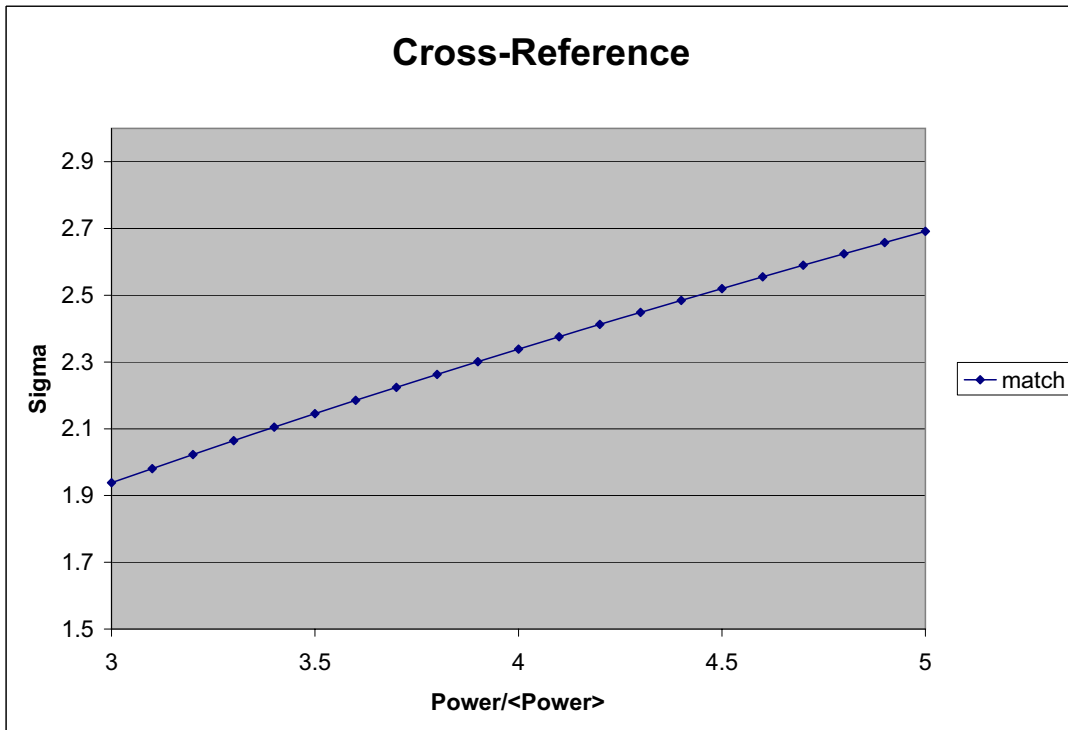

Figure 8: Correspondence of thermal noise voltage fluctuations and corresponding power fluctuation variable: `Power/(average Power)`.
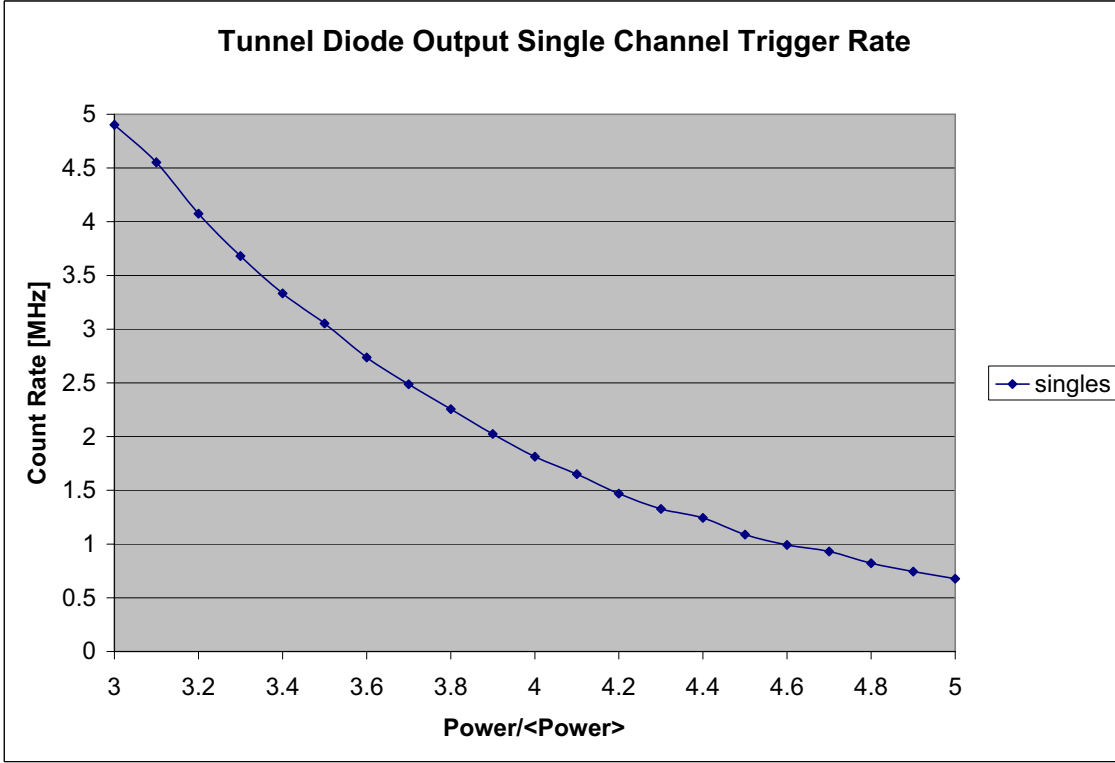
Figure 9: Single channel counting rate as a function of threshold in units of `Power/(average Power)`.

Once a single channel trigger rate r_N is established, subsequent correlations are readily calculable. For a requirement that N channels of M be coincident in a timing interval τ, the rate R for that process may be expressed as:

$$R_{\text{NofM}} = M_N \left(r_N^N \tau^{N-1} \right) \tag{3}$$

where the combinatorics for this process are given by

$$M_N = \frac{M!}{N! \cdot (M - N)!}. \tag{4}$$

Using this prescription, the **Level 1** or antenna trigger rate for 3 of 8 independent bands may be expressed as:

$$R_{\text{3of8}} = \frac{8!}{3! \cdot 5!} \cdot \left(r_N^3 \tau^2 \right) \tag{5}$$

which for a singles rate r_N of 2MHz and τ of 20ns gives a **Level 1** rate:

$$R_{\mathbf{L1}} = 56 \cdot \left(8 \times 10^{18} \cdot (20ns)^2 \right) = 179.2\text{kHz}. \tag{6}$$
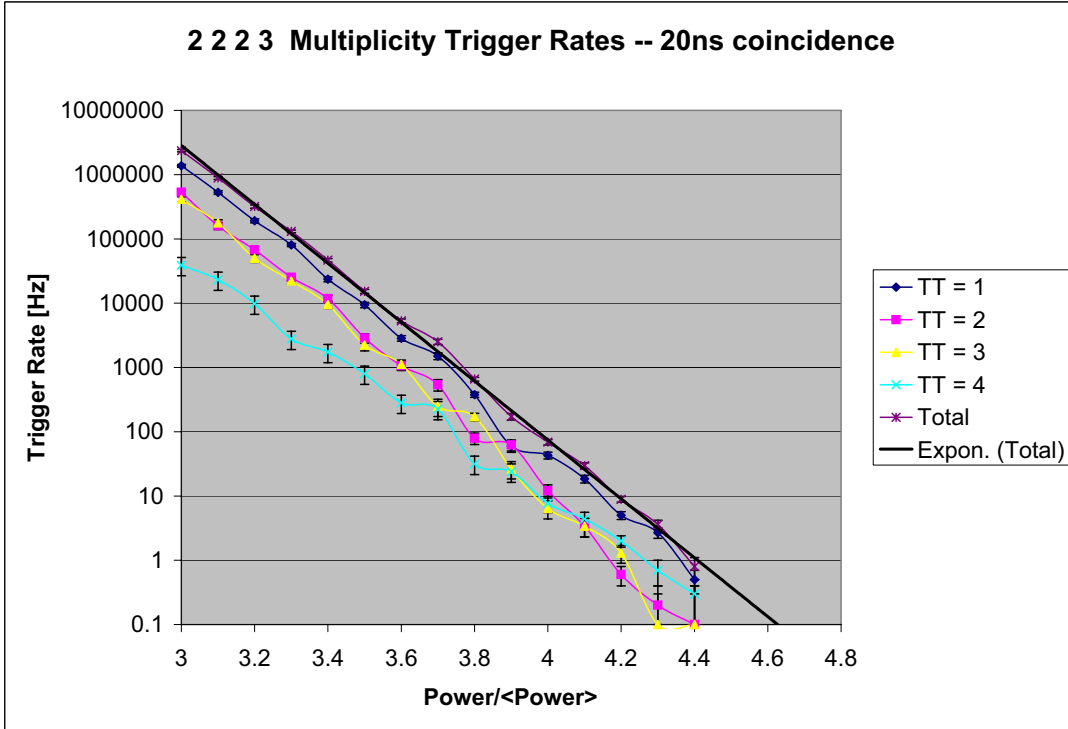
Figure 10: Simulation of the **Level 3** trigger rate by `Trigger Type (TT)` and a sum of these contributions.

3.2 Cluster trigger rates – Level 2

Estimates of local cluster triggers may be constructed by the same means, leading to local trigger rates which may be estimated for the top and bottom as:

$$R_{\mathbf{L2top,bottom}} = 10 \cdot \left(179.2 \mathrm{kHz}^2 \cdot 20ns \right) = 6.42 \mathrm{kHz}. \tag{7}$$

and the rate for the nadir **Level 2** rate is

$$R_{\mathbf{L2nadir}} = 3 \cdot \left(179.2 \mathrm{kHz}^2 \cdot 20ns \right) = 1.93 \mathrm{kHz}. \tag{8}$$

Since random antenna hits can contribute to multiple trigger clusters, the correlations between antenna hits should not be neglected. The simulation takes these possibilities into account. It should be pointed out that these rates are a very strong function of both the single channel rates and coincident overlap, as can be seen in the equations above.

3.3 Global trigger rates – Level 3

Rates for each of the trigger types above may be estimated based upon the overlap probabilities. Because of incident arrival differences due to geometry, a wider **Level 3** window is considered. For this exercise a generous 50ns value was adopted. With this choice, and the logic outlined above, results of the full simulation of the **Level 3** trigger rate as a function of the threshold figure of merit are shown in Figure 10.

9

This is to be compared with the analytical approach above. The 2MHz singles rate chosen above corresponds a Power/(average Power) of about 3.9. Computing the accidental rates for the various trigger types then follows as:

$$R_{\text{TT}=1} = 16 \times R_{\textbf{L2top}} \cdot R_{\textbf{L2bottom}} \cdot 50ns \sim 32Hz \tag{9}$$

where the factor of 16 comes from the 16 ϕ sectors. Likewise for the nadir coincidences:

$$R_{\text{TT}=2} = R_{\text{TT}=3} = 16 \times R_{\textbf{L2top,bottom}} \cdot R_{\textbf{L2nadir}} \cdot 50ns \sim 10Hz \tag{10}$$

Finally, as the timing window and coincidence are the same, the rate for **Level 3** nadir only trigger is the same as that for a single 3 of 3 in a given ϕ sector based on the **Level 1** rate:

$$R_{\text{TT}=4} = \frac{16}{2} \cdot \left(179.2\text{kHz}^3 \cdot (20ns)^2\right) \sim 18\text{Hz}, \tag{11}$$

Note that there is an over-count by a factor of two since there are 8 nadir antennas mapped into 16 ϕ segments, which is corrected for in the coefficient above. As can be seen in comparison with Figure 10, these analytical estimates and the simulation are in good agreement. Given a maximum total trigger rate of 5Hz and a uniform threshold for all channels, the trigger threshold could be set to:

$$\frac{Power}{<Power>} \sim 4.3 \tag{12}$$

for 5Hz operation and a 20ns coincidence window. Since the Power/(average Power) thresholds are independently adjustable, the contribution for each `Trig Type` may be independently adjusted to optimize the balance of triggers. Addition of nadir trigger information allows for trigging of events closer to the ANITA payload, while primary `TT = 1` triggers are most important in terms of observed volume. A detailed study of neutrino sensitivity and expected rates as a function of neutrino energy should help guide this process.

3.4   Possible Threshold Improvement

As mentioned earlier, because the accidental rates depend heavily upon the coincidence window, a huge improvement in accidental noise trigger rate can be had by reducing the coincidence window requirement. Figure 11 demonstrates the dramatic effect of reducing the **L1** and **L2** coincidence windows from 20ns to 10ns. In other words, for an equivalent 5Hz trigger rate, by using this narrower coincidence window, the threshold can be lowered from about 4.3 to 3.6 in Power/(average Power), allowing for operation more deeply into the noise and improving the GZK neutrino detection sensitivity.

Comparing with the 2.3 σ noise voltage sensitivity used in the ANITA reach Monte-Carlo, it is seen that this corresponds in the ideal case to a Power/(average Power) of about 3.9, which is in between the two simulation cases shown. Equivalently, this is comparable to an overlap coincidence of something like 15ns. Through careful cable and trace length management and the use of pipelined logic, with an effective 4ns clock edge (125 MHz, both edges), a coincidence window of 12-16ns should be easily achievable. Also the 50ns **Level 3** coincidence window considered above is probably far too wide, as it is much larger than any realistic incident signal timing difference, and tightening this would help further reduce the accidental trigger rate. Maintaining a fixed trigger rate, this will permit operation at even lower trigger thresholds.
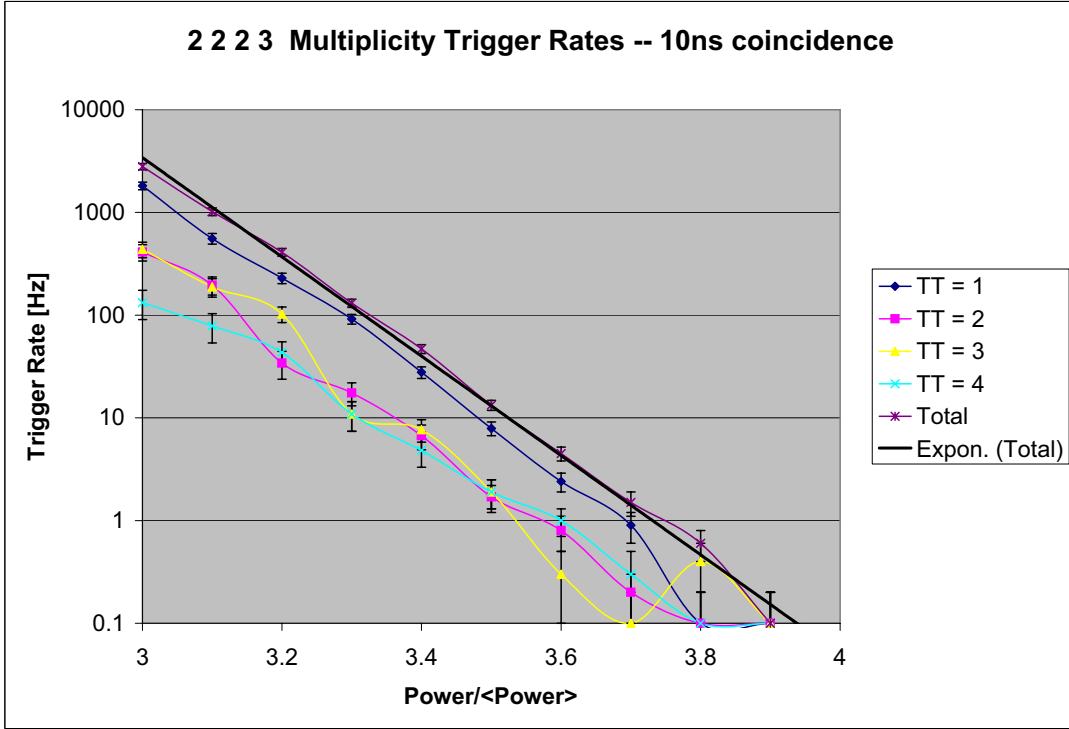
Figure 11: Simulation for the same trigger configuration as Figure 10, but with a 10ns single antenna (**Level 1**) and cluster coincidence (**Level 2**) timing window.

4 Payload and External Noise

As the estimates above indicate, operation at well into the thermal noise is possible while retaining acceptably small trigger rates. However, it should be noted that thermal noise fluctuations are not the only source of background triggers. In particular this analysis does not provide a means of estimating the sensitivity to locally induced (payload) noise, or anthropogenic noise sources. The global trigger logic needs to be flexible enough to provide pattern rejection based upon backgrounds seen in ground tests, as well as those observed while in flight. Adopting a two-tier `Hold` and `Digitize` processing scheme allows for a significant amount of pattern processing while incurring essentially no additional deadtime.

An example of such a pattern match would be the rejection of trigger events which trigger opposite `Trig Type = 1` ϕ sectors at precisely the same time – clearly consistent with noise originating from the payload. A simulation study of the signatures for such backgrounds will be undertaken as part of the development of such rejection algorithms.

5 Summary

A detailed description of the baseline ANITA trigger hierachy has been presented. Monte Carlo simulations and analytic calculations of the ANITA thermal noise trigger rates, at the noise thresholds used in GZK neutrino sensitivity simulations, are shown to be manageable. The proposed architecture provides substantial flexibility in maintaining uniform trigger rates while providing robust rejection of backgrounds.

References

[1] ANITA Concept Study Report to the NASA Small Explorers Program. Draft available online: http://www.phys.hawaii.edu/∼gorham/ANITA/AnitaCSR.pdf

[2] G.A. Askaryan, *JETP* **14**, 441 (1962); also *JETP* **21**, 658 (1965).

[3] P.W. Gorham, K.M. Liewer, C.J. Naudet, D.P. Saltzberg, and D. Williams, "Radio limits on an isotropic flux of ≥100 EeV cosmic neutrinos," Proc. RADHEP 2000, ed. D. Saltzberg & P. Gorham, (Amer. Inst. Phys. press), in press, (2001); astro-ph/0102435.

[4] ANITA-Lite Trigger Object (ALTO Rev. B) User's Manual, G. Varner *et al.*, available online: http://www.phys.hawaii.edu/∼idlab/project_files/anita/docs/ALTOREVB_manual.pdf

[5] The `LGT_sim.c` program: http://www.phys.hawaii.edu/∼varner/LGT_sim.c